Desalination and Water Treatment
www.deswater.com

doi: 10.5004/dwt.2018.21827

102 (2018) 253–263
January

One-pot solvothermal preparation of ethylenediamine-functionalized nanochain and its adsorption-in situ degradation of 2,4,6-trichlorophenol

Mei-Qin Hu, Hao-Yu Shen*, Zhe-Hao Jiang, Yu-Fei Wang, Le-Yi Weng, Qi Jiang

Ningbo Institute of Technology, Zhejiang University, Ningbo, Zhejiang 315100, China, Tel. +86 574 88130130; emails: hyshen@nit.zju.edu.cn (H.-Y. Shen), mqhu@nit.zju.edu.cn (M.-Q. Hu), 1565680974@qq.com (Z.-H. Jiang), 2191983057@qq.com (Y.-F. Wang), 1102325480@qq.com (L.-Y. Weng), 1061359460@qq.com (Q. Jiang)

Received 30 July 2017; Accepted 19 December 2017

ABSTRACT

An ethylenediamine (EDA)-functionalized Fe_3O_4 magnetic nanochain (EDA@*n*Fe_3O_4) was synthesized by one-pot solvothermal method. The EDA@*n*Fe_3O_4 was characterized by elementary analysis, powder X-ray diffraction, Fourier transform infrared spectroscopy, transmission electron microscopy, and vibrating sample magnetometer. Its application for adsorption and degradation of 2,4,6-trichlorophenol (2,4,6-TCP) was investigated. The results show that the EDA@*n*Fe_3O_4 has an average size of ~150 nm, and self-assembled to be a nanochain, with the saturation magnetization intensity of 46.8 emu/g. The adsorption capacity of EDA@*n*Fe_3O_4 is found to be 902.5 mg/g when the initial concentration of 2,4,6-TCP at 1,000 mg/L. The adsorption processes fit the Freundlich isotherms well. The adsorption processes reach the equilibrium within 5 min and the kinetic data are well fitted to the pseudo-second-order model. The post-adsorbed material was added to Fe^{3+}–H_2O_2 system. In situ degradation of 2,4,6-TCP via Fenton-like reaction under visible light can be realized. The results indicate that at pH 3.0–8.0, the degradation of 2,4,6-TCP with loading concentration at 6.20–122.2 mg/g can be reached to almost 100% within 5 min. EDA@*n*Fe_3O_4 can be reused after regeneration. It is a potential effective and reusable material for adsorption and degradation of 2,4,6-TCP.

Keywords: Ethylenediamine (EDA)-functionalized nanochain (EDA@*n*Fe_3O_4); 2,4,6-TCP; Adsorption; In situ degradation

1. Introduction

Chlorophenols (CPs) are widely used pesticides, disinfectants, wood preservatives, and pulp bleaching agents [1], resulting in the release of CPs into the environment. Because of their high toxicity to aquatic life, persistence and bioaccumulation potential, some of CPs, such as 2,4-dichlorophenol, 2,4,6-trichlorophenol (2,4,6-TCP), and pentachlorophenol have been regulated as priority pollutants by the US Environmental Protection Agency (EPA), European Commission (EC) Environmental Directive (2455/2001/EC) and China [2]. Attention has been paid to develop an effective approach for the treatment of CPs contained wastewater in recent years. Among the potential effective treatment technique, the development of new adsorbents for effective removal and separation of CPs in environmental matrices is of particular significance.

Some kinds of adsorbents for CPs contained wastewater treatment have been developed, such as activated carbon [3,4], fiber composites [5], resins [6], biochar [7], and molecularly imprinted polymers [8]. Recently, Fe_3O_4-based magnetic nanoparticles (MNPs) have found to be simple, convenient, and powerful approaches for the separation and purification of environmental samples, and removal of toxic pollutants in water [9–15]. Although such MNPs possess unique magnetic

* Corresponding author.

properties and can be separated simply from the solution by a magnetic field, how to treat the post-adsorption material is still facing great challenge.

Advanced oxidation processes (AOPs) have been proposed as offering promise for CPs pollutant treatment [16]. Among AOPs, oxidation using Fenton's reagent is an attractive treatment for the effective degradation of CPs because of its low cost, the lack of toxicity of the reagents [17].

It would be desirable if three of the promising concepts (high adsorption capacity, magnetic separation, and effective degradation) were combined. Herein, we reported the design and successful synthesis of an ethylenediamine (EDA)-functionalized nano-Fe_3O_4 magnetic chain (EDA@*n*Fe_3O_4). It was synthesized via one-pot solvothermal method, for effective adsorption and in situ degradation of 2,4,6-TCP via Fenton-like reaction under visible light. The three-in-one system not only provides EDA@*n*Fe_3O_4 with high adsorption capacity but also extends the catalytic potential of MNPs. The superparamagnetism of the incorporated Fe_3O_4 nanoparticles allows magnetic separation to replace the centrifugation and filtration step in a convenient and economical way. The presumed mechanism for high adsorption properties and in situ degradation of 2,4,6-TCP of the as-prepared EDA@*n*Fe_3O_4 nanochain was deeply investigated in present work. The overall procedure of the present work was shown in Fig. 1.

2. Experimental

2.1. Materials

Ferric chloride ($FeCl_3·6H_2O$), sodium acetate (NaAc), ethylene glycol (EG), 30% hydrogen peroxide solution (H_2O_2), *tert*-butanol (tBu-OH), disodium ethylenediaminetetraacetate (Na_2-EDTA) and benzoquinone were analytical grade, and purchased from Sinopharm Chemical Reagent Co., Ltd. (Shanghai, China). EDA and 2,4,6-trichloropyridine (2,4,6-TCP) were supplied by Aladdin Chemical Reagent Co., Ltd. (Shanghai, China). LC grade of methanol, acetonitrile, and ammonium acetate (NH_4Ac) were obtained from Merck (Darmstadt, Germany). Distilled water was used to prepare all the solutions. HCl (0.1 mol/L) and NaOH (0.1 mol/L) solutions were used for pH adjustment.

2.2. Preparation of EDA@*n*Fe_3O_4

The overall preparation of EDA-functionalized nano-Fe_3O_4 magnetic composite material (EDA@*n*Fe_3O_4) was produced using a polyol-media one-pot solvothermal method. The 4.0 g of $FeCl_3·6H_2O$ and 12.0 g of NaAc were dissolved in 120 mL EG. This solution was stirred vigorously at room temperature for 10 min to form a stable orange solution. EDA (40 mL) was then added with constant stirring for 30 min until

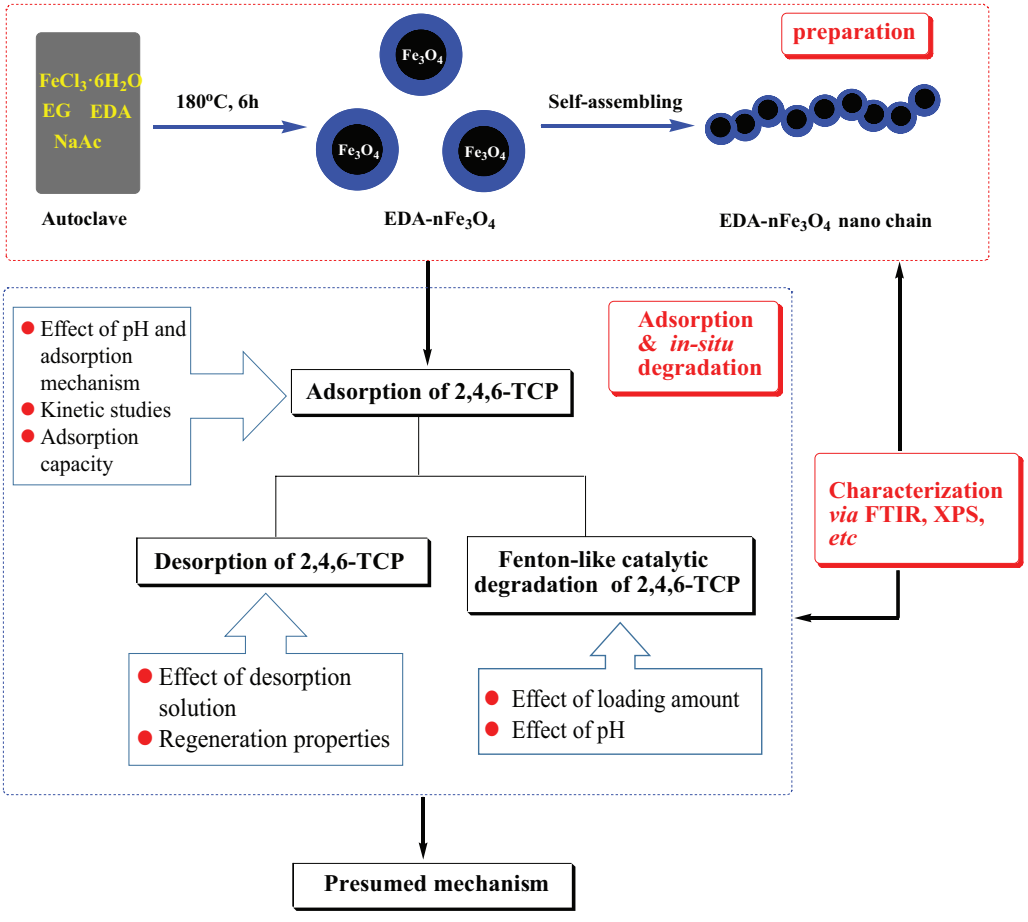

Fig. 1. Overall procedure of the EDA@nFe_3O_4 nanochain preparation and its adsorption-in situ degradation of 2,4,6-TCP.

completely dissolved. The mixture solution was then transferred to a Teflon-lined autoclave and heated at 180°C for 8 h. After the autoclave cooled to room temperature, the resulting EDA@$n$$Fe_3O_4$ was isolated under magnetic field and washed with water and ethanol to remove redundant reagents and impurities. The as-prepared EDA@$n$$Fe_3O_4$ was dried in a vacuum oven at 60°C for 12 h and stored in a sealed bottle for further use. The synthesis of nano-Fe_3O_4 was also carried out in similar procedures described above without the adding EDA.

2.3. Characterization

The morphology and dimensions of the synthesized EDA@$n$$Fe_3O_4$ were examined by transmission electron microscopy (TEM; Hitachi H-7650) at 80 kV. Each sample was prepared by placing a very dilute particle suspension onto 400 mesh carbon grids coated with copper film. Scanning electron microscopy (SEM) was performed using scanning electron microscopy (SEM, JSM-6700F) at an accelerating voltage of 5.0 kV. Sample dispersed at an appropriate concentration in ethanol was cast onto a silicon sheet at room temperature and sputter-coated with gold. Magnetic behavior was analyzed by a vibrating sample magnetometer (VSM; Lake Shore 7410). The structures of EDA@$n$$Fe_3O_4$ were determined by an X-ray diffractometer (XRD; Bruker D8 Advance) at ambient temperature. The instrument was equipped with a copper anode generating Cu Ka radiation (λ = 1.5406 Å). Fourier transform infrared spectroscopic (FTIR) spectra were recorded on a Thermo Nicolet (NEXUS-470) FTIR spectrometer. Nitrogen percentage of EDA@$n$$Fe_3O_4$ was analyzed with an elemental analyzer (ThermoFisher Flash-1112). Fe_3O_4 percentage was calculated via the content of the Fe of EDA@$n$$Fe_3O_4$, which was obtained by detection of iron ions using a spectrophotometer (722, Shanghai, China) according to the standard colorimetric method [18]. The concentration of 2,4,6-TCP in the aqueous solution was analyzed by HPLC method. The HPLC analysis was performed on an Elite HPLC system including a binary pump and a UV detector (Elite Corporation, PRC), using a ZORBAX SB-C8 (5 μm particle size, 250 mm × 4.6 mm) analytical column. The mobile phase was using a 70:30 methanol and 5 mmol/L NH_4Ac aqueous solution (v/v), at a flow rate of 1.0 mL/min. The analytes were detected by diode array detector at 230 nm. Column was maintained at a temperature of 35°C to enhance the retention time reproducibility, and the injection volume was 20.0 μL.

2.4. Adsorption experiments

Batch adsorption experiments were carried out in 150 mL stoppered flasks, each of which contained 40 mL of 2,4,6-TCP solution. A 20 mg amount of EDA@$n$$Fe_3O_4$ was added into each flask and shaken at 180 rpm in a thermostatic shaker. The solution pH was adjusted by 0.1 mol/L HCl or 0.1 mol/L NaOH solution. The 2,4,6-TCP concentration in the supernatant was measured by HPLC analysis. According to the 2,4,6-TCP concentrations before and after adsorption, the equilibrium adsorption capacity (q, mg/g) of 2,4,6-TCP bound to the EDA@$n$$Fe_3O_4$ is calculated using Eq. (1) [19]:

$$q = \frac{(C_0 - C_e)V}{m} \tag{1}$$

where C_0 and C_e represent the initial solution concentration and the equilibrium concentration of 2,4,6-TCP (mg/L), V is the volume of the 2,4,6-TCP solution (mL), and m is the adsorbent dosage (mg), the same hereinafter.

To investigate the effect of pH, 40 mL of 50, 200, and 500 mg/L 2,4,6-TCP with pH ranging from 2.0 to 10.0 were mixed with 20 mg of magnetic adsorbents for 30 min at 308 K, respectively. In the kinetic experiments, the EDA@$n$$Fe_3O_4$ was also investigated with contacting time ranging from 1 to 180 min. The pseudo-first-order model (Eq. (2)) [19], pseudo-second-order model (Eq. (3)) [19–21], and intraparticle diffusion model (Eq. (4)) [19] were used to fit the experimental data.

$$\log(q_e - q_t) = \log q_e - \left(\frac{k_1}{2.303}\right)t \tag{2}$$

$$\frac{t}{q_t} = \frac{1}{k_2 q_e^2} + \left(\frac{1}{q_e}\right)t \tag{3}$$

$$q_t = k_{id}t^{1/2} + C \tag{4}$$

where q_e and q_t are the adsorption capacities at equilibrium and at time t (mg/g), respectively. k_1 (min^{-1}) and k_2 (g/(mg min)) are the adsorption rate constants, k_{id} is the intraparticle diffusion rate constant (mg/(g $min^{-1/2}$)), and C is the intercept (mg/g).

The adsorption isotherm studies were investigated with 2,4,6-TCP initial concentration ranging from 5 to 1,000 mg/L at 308 K for 1 h. Two adsorption isotherms, Langmuir model (Eq. (5)) [19,22] and Freundlich model (Eq. (6)) were applied to analyze the adsorption data [19,23].

$$\frac{C_e}{q_e} = \frac{1}{K_L q_m} + \frac{C_e}{q_m} \tag{5}$$

$$\log q_e = \log K_F + (1/n)\log C_e \tag{6}$$

where q_m and K_L are the Langmuir constants related to the maximum adsorption capacity and apparent heat change, respectively, while K_F is a Freundlich constant related to adsorption capacity and 1/n is a Freundlich constant related to the adsorption intensity.

2.5. Fenton-like catalytic degradation investigation

The post-adsorbed material was isolated under magnetic field and dispersed to 10 mL acetonitrile. 100 μL of 10^{-3} mol/L Fe^{3+} solution, 20 μL of 30% H_2O_2 was then added. The mixture was shaken at 150 rpm in a thermostatic shaker. Sampling at every 1 min, followed by adding one drop of 10% Na_2SO_3 solution to stop the reaction. 1% NaOH methanol solution was used for the desorption of the 2,4,6-TCP on the EDA@$n$$Fe_3O_4$. HPLC method was applied for the residue 2,4,6-TCP concentrations of both the post-catalytic reaction solution and the desorption solution. The degradation rates of 2,4,6-TCP

under different loading amount and different pH conditions were calculated according to Eq. (7):

$$D = \frac{A_0 - A_t}{A_0} \times 100\% \quad (7)$$

where D is the degradation rate of 2,4,6-TCP; A_t and A_0 are the HPLC peak area of 2,4,6-TCP at time t and at time 0, respectively.

2.6. Desorption and regeneration investigation

Desorption experiments were carried out with the 2,4,6-TCP post-adsorption EDA@nFe$_3$O$_4$ samples, extracted with 1 mL 1% NaOH methanol solution, shaken at 180 rpm in a thermostatic shaker for two times. The recoveries of 2,4,6-TCP were determined by HPLC analysis. The post-desorption materials were isolated under magnetic field and washed with water and ethanol, dried in a vacuum oven at 60°C for 12 h for regeneration investigation. The regeneration experiments were carried out according to the adsorption experiments as described in section 2.4.

3. Results and discussion

3.1. Characterization of EDA@nFe$_3$O$_4$

The SEM and TEM images of EDA@nFe$_3$O$_4$ were shown in Fig. 2. All size data reflect the averages of about 100 particles and are calculated according to Eq. (8) [24]:

$$U = D_w/D_n, \quad D_n = \sum_{i=1}^{k} n_i D_i / \sum_{i=1}^{k} n_i, \quad D_w = \sum_{i=1}^{k} n_i D_i^4 / \sum_{i=1}^{k} n_i D_i^3 \quad (8)$$

where U is the polydispersity index, D_n is the number-average diameter, D_w is the weight-average diameter, and D_i is the diameter of the determined microspheres. It revealed that the EDA@nFe$_3$O$_4$ particles were multidispersed with an average diameter of around 150 nm (Figs. 2(a) and (b)), and self-assembled as a nanochain (Fig. 2(c)).

The paramagnetic properties of the EDA@nFe$_3$O$_4$ were verified by the magnetization curve measured by VSM shown in Fig. 3(a). The saturation moment obtained from the hysteresis loop was found to be 46.8 emu/g. The EDA@nFe$_3$O$_4$ nanochain was expected to respond well to magnetic fields without any permanent magnetization, therefore, making the solid and liquid phases separate easily. Interestingly, the saturation moment of the present nanochain was much higher than those of our previously reported EDA-functionalized nanomagnetic polymers (EDA@NMPs), which ranged from 12.3 to 5.56 emu/g [25]. It might be due to two facts: (1) antimagnetic polymer anchored onto the Fe$_3$O$_4$ core of the NMPs, which leading a decrease of content percentage of Fe$_3$O$_4$ in the NMPs; (2) the ordered structure of the nanochain might be favorable to magnetic ordering, which leading an increase of the saturation moment.

To further demonstrate the crystal structure of EDA@nFe$_3$O$_4$, the XRD patterns of the as-prepared Fe$_3$O$_4$ (without adding EDA) and EDA@nFe$_3$O$_4$ were collected (Fig. 3(b)).

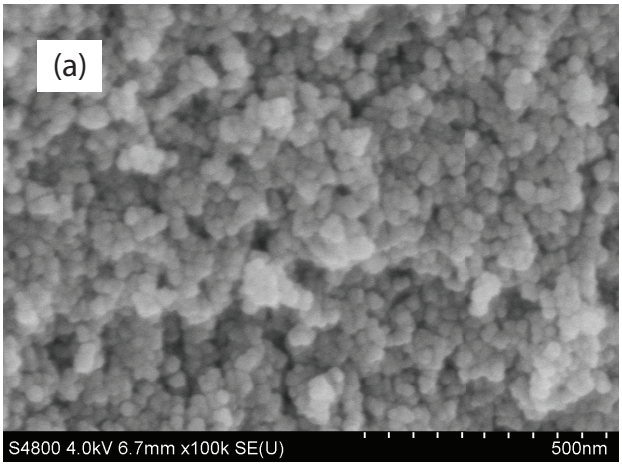

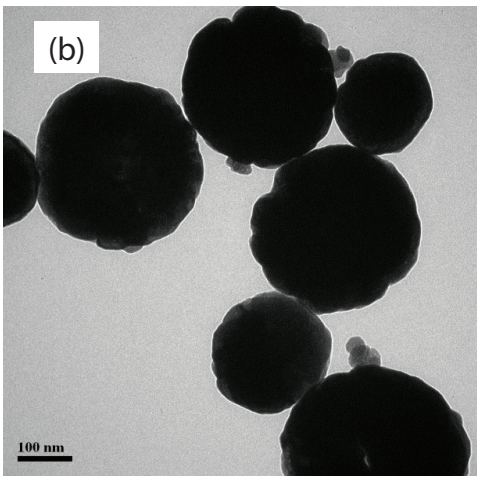

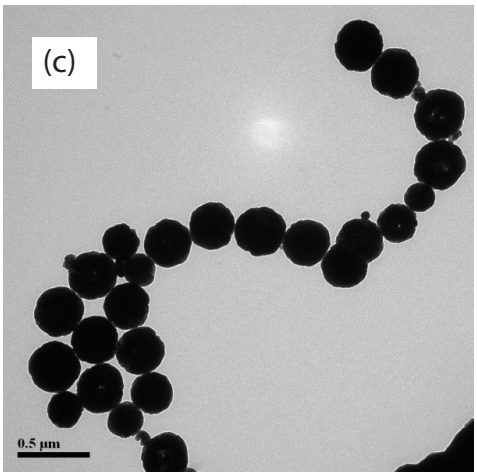

Fig. 2. (a) SEM and (b) and (c) TEM images of EDA@nFe$_3$O$_4$.

It indicated that EDA@nFe$_3$O$_4$ had retained the spinel structure of Fe$_3$O$_4$, in which the identical peaks for Fe$_3$O$_4$ located at 30.1°, 35.5°, 43.1°, 53.4°, 57.0°, and 62.6°, corresponding to their indices (220), (311), (400), (422), (511), and (400) appeared [25]. The intensity of diffraction peaks became slightly weaker with the amino-function and the formation of the nanochain.

Elemental analysis results showed that nitrogen percentage of EDA@nFe$_3$O$_4$ was 15.8%, while the total content of Fe$_3$O$_4$ in the EDA@nFe$_3$O$_4$ was 56.8%, which was higher than those of our previously reported NMPs, and consisted with the VSM results.

3.2. Adsorption of the EDA@nFe$_3$O$_4$ to 2,4,6-TCP

3.2.1. Effect of pH and adsorption mechanism

The effect of solution pH was investigated with the pH values ranging from 2.0 to 10.0, with the initial concentration of 2,4,6-TCP at 50, 200, and 500 mg/L, respectively, and the results are shown in Fig. 4. The adsorption capacity of 2,4,6-TCP was dependent on solution pH. With the solution pH increasing, the adsorption capacities first increased with the solution pH ranging from 2.0 to 4.0, and reached a plateau value with pH ranging from 4.0 to 8.0, then decreased at the pH > 8.0. The dependence of 2,4,6-TCP adsorption on solution pH could be explained from the perspectives of surface charge of the adsorbent and the state of 2,4,6-TCP at various pH values. As the pKa of 2,4,6-TCP is at 6.0–7.4 [26], under acidic conditions (pH < 4.0), the amino groups on the surface of EDA@nFe$_3$O$_4$ are easy to be protonated, and the main formation was –NH$_3^+$ without lone pair electrons and it was difficult to form hydrogen bond (–O–H···N) with 2,4,6-TCP (Fig. 5(a)). At pH ranging from 4.0 to 8.0, the main formation of the surface groups might be –NH$_2$. Hydrogen bond (–O–H···N) formed to obtain the highest adsorption capacity of 2,4,6-TCP (Fig. 5(b)). When pH > 8.0, OH$^-$ ions may be adsorbed to the surface of EDA@nFe$_3$O$_4$ (Fig. 5(c)), which contributed to the negatively charged sites of the EDA@nFe$_3$O$_4$. Meanwhile, 2,4,6-TCP molecules presented in an ionic state (deprotonation of hydroxyl group, –O$^-$), and there would be repulsion between these sites and the deprotonation state of 2,4,6-TCP, finally resulted in difficulties to form hydrogen bonds (–O–H···N) with amino groups on the surface of EDA@nFe$_3$O$_4$ (Fig. 5(c)). The scheme of adsorption mechanism was shown in Fig. 5.

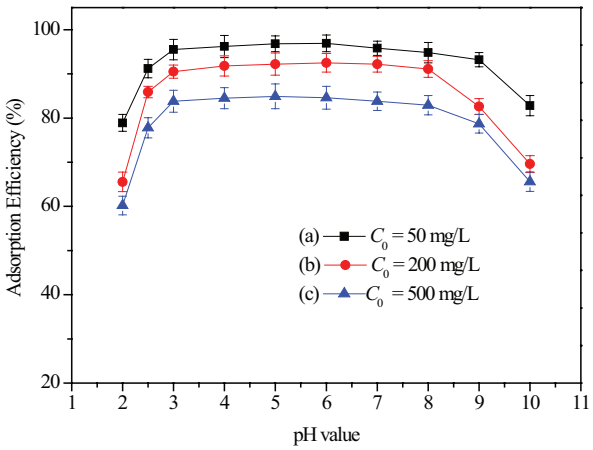

Fig. 4. The pH effect on the adsorption of 2,4,6-TCP solutions at concentration of: (a) 50 mg/L, (b) 200 mg/L, and (c) 500 mg/L.

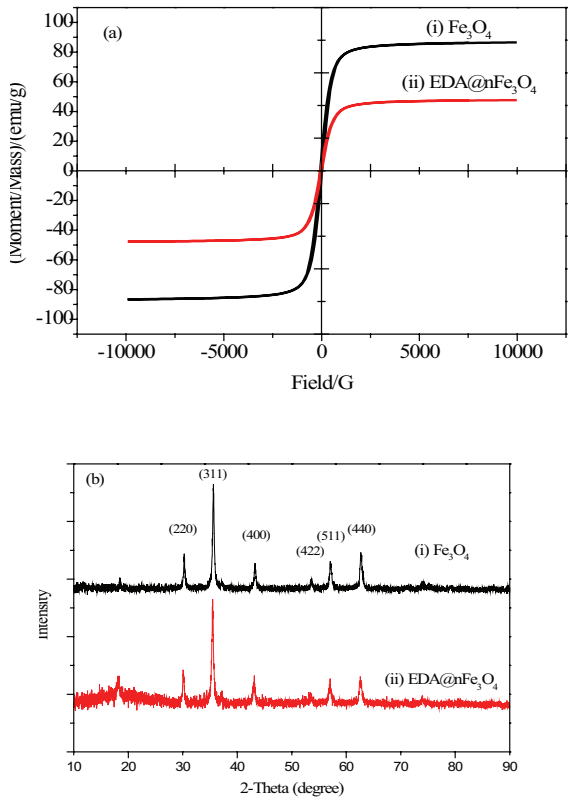

Fig. 3. (a) VSM and (b) XRD characterization of EDA@nFe$_3$O$_4$.

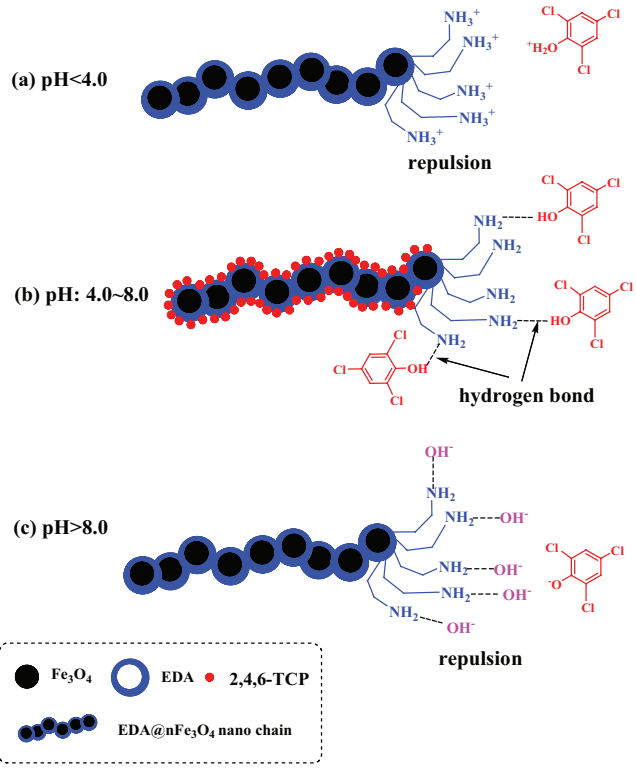

Fig. 5. Probable adsorption mechanism of 2,4,6-TCP on the EDA@nFe$_3$O$_4$ under different pH value.

The adsorption mechanism could be confirmed by X-ray photoelectron spectroscopy (XPS) and FTIR analyses of EDA@nFe$_3$O$_4$ before and after 2,4,6-TCP adsorption (Fig. 6). From the survey scan of XPS spectra (Fig. 6(a)), a new peak owing to Cl2p could be observed after 2,4,6-TCP loaded on EDA@nFe$_3$O$_4$, indicating the successful adsorption of 2,4,6-TCP. The N1s high-resolution scan of EDA@nFe$_3$O$_4$ could be deconvoluted into two individual peaks at binding energies of 398.5 and 396.6 eV (Fig. 6(b)), which were assigned to the N atoms in C–N and –NH$_2$ groups of EDA [27], respectively. A new peak at 399.6 eV was observed after 2,4,6-TCP adsorption, which could be attributed to the hydrogen bonding of

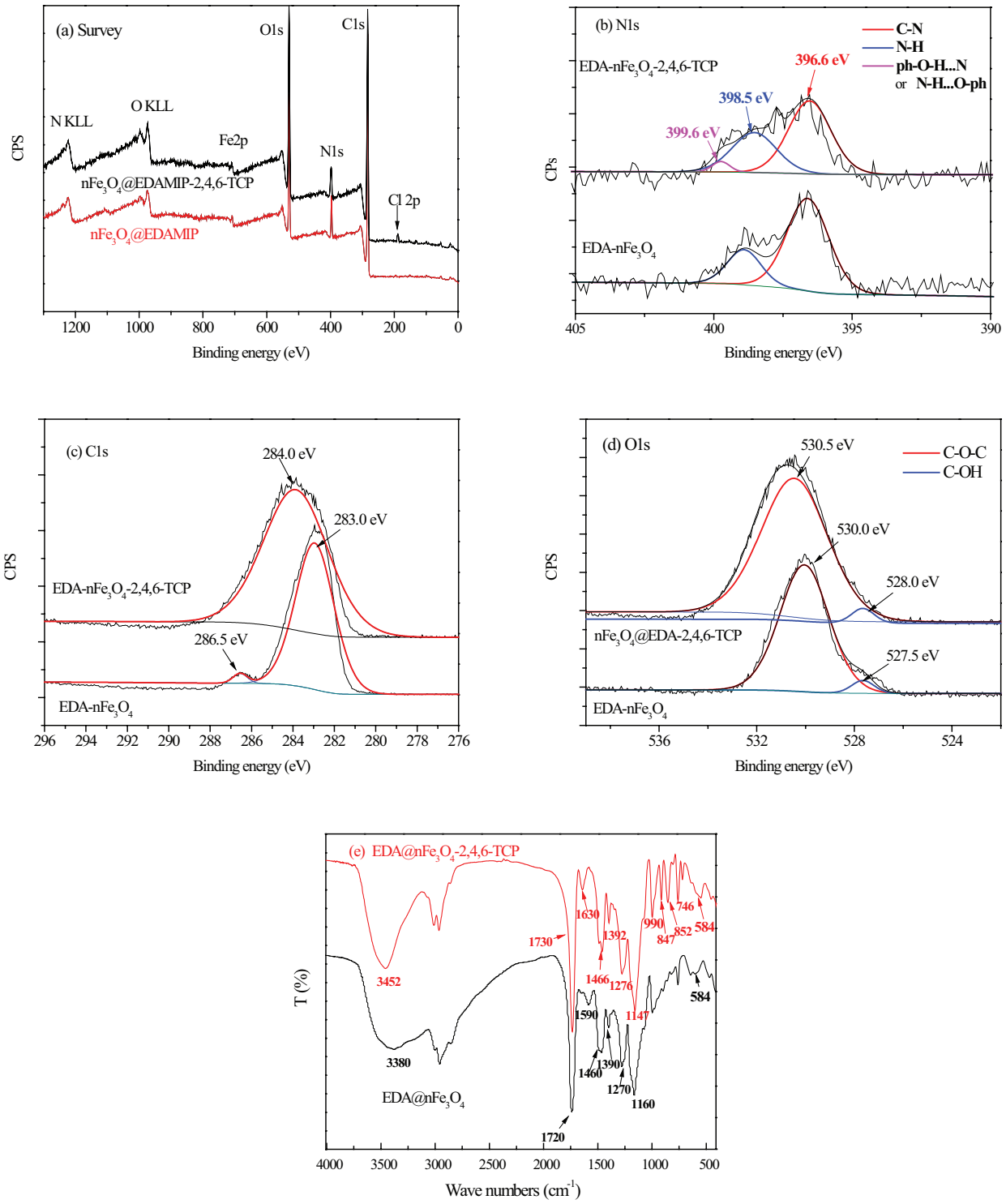

Fig. 6. XPS spectra of (a) survey scan, and high-resolution scan of: (b) N1s; (c) C1s; (d) O1s; (e) FTIR spectra of EDA@nFe$_3$O$_4$ and EDA@nFe$_3$O$_4$-2,4,6-TCP.

ph–O–H···NH_2 or –N–H···O–ph [28]. In the XPS spectra of C1s (Fig. 6(c)), the carbon atoms can be found in two chemically different positions, leading to two differing C1s binding energies: C–C (~283.0 eV) and C–N (~286.5 eV). After adsorption, only one peak at ~284.0 eV with a broader band range appeared, which may attribute to the involvement of the –NH_2 groups of EDA in the adsorption of 2,4,6-TCP. Similar phenomena were observed in the XPS spectra of O1s (Fig. 6(d)), the peaks of O1s appeared at ~530.5 eV, assigned to C–O–C and C–OH groups, broadening with a slight shift of binding energies after adsorption of 2,4,6-TCP.

The IR spectra of EDA@$n$$Fe_3O_4$ before and after adsorption of 2,4,6-TCP were showed in Fig. 6(e). The broad peak appeared at ~3,380 and ~1,590 cm^{-1} can be assigned to be the stretching and bending vibrations of the –NH and –NH_2 groups. While after adsorption, the broad peak appeared at ~3,380 cm^{-1} became sharper, and shifted to ~3,452 cm^{-1}, while the characteristic bands at ~1,590 cm^{-1} disappeared along with the appearance of the bands at ~1,630 cm^{-1}, which may be attributed to the interaction between amino groups and the 2,4,6-TCP, indicating that the hydrogen bonds (–N–H···O) were formed between –NH_2 groups and 2,4,6-TCP subsequently weakened the N–H bonding and resulted in a large shift (40–70 cm^{-1}) [29]. A group of new peaks located at 746–990 cm^{-1} can be clearly observed after 2,4,6-TCP loaded on EDA@$n$$Fe_3O_4$, which was attributed to the stretching vibration of C–Cl bond and the skeleton vibration absorption of benzene rings [30,31].

3.2.2. Kinetic studies

Fig. 7(a) presents the adsorption kinetics of 2,4,6-TCP onto EDA@$n$$Fe_3O_4$. The adsorption capacities increased rapidly and reached equilibrium in 5, 10, and 20 min, with the initial concentration of 2,4,6-TCP at 50, 200, and 500 mg/L, respectively, which were much faster than those in Shen et al. [14]. Unlike previously reported magnetic polymers ($n$$Fe_3O_4$@$NH_2$MIP), nano-$Fe_3O_4$ in present adsorbent was surface-engineered by EDA directly, without polymer matrix, the target adsorbate, 2,4,6-TCP, could reach the surface of in adsorbent fast, and shorten the equilibrium time.

The mechanism for 2,4,6-TCP removal by adsorption on EDA@$n$$Fe_3O_4$ might involve the following four main steps: (i) migration of 2,4,6-TCP from bulk of the solution to the surface of the adsorbent (bulk diffusion); (ii) diffusion of 2,4,6-TCP through the boundary layer to the adsorbent (film diffusion); (iii) transport of 2,4,6-TCP from the surface to the particle (intraparticle diffusion); and (iv) adsorption of 2,4,6-TCP at an active site on the surface of material.

For the intraparticle diffusion model [32], if the regression of q_e vs. $t^{1/2}$ is linear and passes through the origin, then the sole rate-limiting step is intraparticle diffusion, otherwise not [33]. By the plotting of q_t vs. $t^{1/2}$, bilinearities were observed (shown in Fig. 7(b)), suggesting that the intraparticle diffusion was not the only rate-limiting step, other processes might also be involved. As shown in Fig. 7(b), two steps might take place in the present system. The first sharp portion (k = 12.33, 125.75, and 196.81 for the initial concentration of 2,4,6-TCP at 50, 200, and 500 mg/L, respectively) related to the diffusion of 2,4,6-TCP from the solution to the external surface of the EDA@$n$$Fe_3O_4$ (step (i)), or the boundary layer

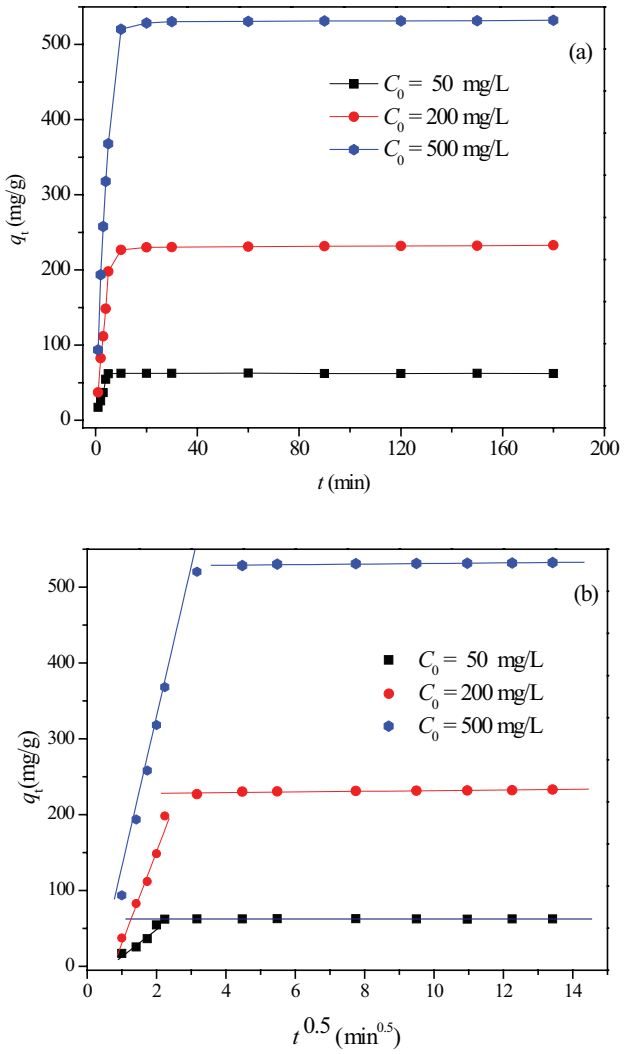

Fig. 7. Effect of adsorption time on the adsorption of 2,4,6-TCP onto EDA@$n$$Fe_3O_4$.

diffusion of 2,4,6-TCP in the solution (step (ii)). The second linear portion was attributed to the final equilibrium stage (step (iv)). The intraparticle process might not be involved in the rate-limiting steps [32]. In our present study, the first two steps (bulk diffusion and film diffusion) could be eliminated by shaking, and that might be the reason why the slope of the first portion was sharp and the initial adsorption rate was quite high. Therefore, in the present case, 2,4,6-TCP reached the surface amino functional groups of EDA@$n$$Fe_3O_4$ easily and took less time to reach adsorption equilibrium, implying that the surface grafting of amino groups of EDA@$n$$Fe_3O_4$ allowed efficient mass transport, thus overcoming some drawbacks of traditional materials.

Pseudo-first-order and pseudo-second-order models were used to describe the adsorption kinetic data. The correlation coefficient values indicated a better fit of the pseudo-second-order model with the experimental data compared with the pseudo-first-order for EDA@$n$$Fe_3O_4$. The equations and constants, including k_2, $q_{e,cal}$, and initial adsorption rates ($k_2q_e^2$) calculated from the equation, are listed in Table 1. The data exhibit good linearities for all the adsorbents

with R^2 above 0.9995. The calculating equilibrium adsorption capacity ($q_{e,cal}$) from the pseudo-second-order model was very close to the experimental (q_e). For different initial concentration of 2,4,6-TCP, the adsorption rate constants (k_2) kept almost constant at around 0.015 g/(mg min). It was worth to be noted that with the initial concentration of 2,4,6-TCP increased, the initial adsorption rates ($k_2q_e^2$) increased, 60.6, 833.3, and 4,545 mg/(g min), for the initial concentration of 2,4,6-TCP at 50, 200, and 500 mg/L, respectively. This results indicated that with the increasing of the initial concentration of 2,4,6-TCP, the probability of a collision between the 2,4,6-TCP and the surface amino functional groups of EDA@nFe$_3$O$_4$ was high, leading a faster reaction rate.

3.2.3. Adsorption capacity of EDA@nFe$_3$O$_4$

The adsorption capacity of EDA@nFe$_3$O$_4$ to 2,4,6-TCP was investigated by varying the initial concentration of 2,4,6-TCP solutions from 5.0 to 1,000 mg/L. Fig. 8 shows that the adsorption capacities of EDA@nFe$_3$O$_4$ to 2,4,6-TCP increased almost linearly with the increase of initial concentration of 2,4,6-TCP, did not reach an equilibrium even at C_0 = 1,000 mg/L. The adsorption capacity of EDA@nFe$_3$O$_4$ is found to be 902.5 mg/g when the initial concentration of 2,4,6-TCP at 1,000 mg/L. Although the represented parameters fit both Langmuir and Freundlich adsorption models well. The Freundlich model could more effectively describe the adsorption data with a higher R^2 (=0.997) than that of Langmuir adsorption model (R^2 = 0.933), which suggested a multilayer adsorption. Table 2 presents the isotherm parameters as well as the correlation coefficients (R^2) of the adsorption data in the equations. The 1/n values of EDA@nFe$_3$O$_4$ were between 0 and 1, indicating the heterogeneity of their surface with exponential distribution of energy of active sites.

3.3. In situ degradation of 2,4,6-TCP on post-adsorption EDA@nFe$_3$O$_4$

A series of post-adsorption EDA@nFe$_3$O$_4$ with the initial concentration at 5.00–300.0 mg/L 2,4,6-TCP, in which the adsorption efficiency was over 90% and the adsorption capacity (i.e., loading amount) was at 6.20–342.4 mg/g, were magnetic separated, then were dispersed into 10 mL acetonitrile, followed by adding 100 μL of Fe^{3+} solution at concentration of 10^{-3} mol/L, and 20 μL of 30% H_2O_2. The mixture was shaken at 150 rpm in a thermostatic shaker. Sampling at every 1 min, then followed by adding one drop of 10% Na_2SO_3 solution to stop the reaction. The effect of solution pH was investigated with the pH values ranging from 2.0 to 10.0, for the post-adsorption EDA@nFe$_3$O$_4$ with loading amount 6.20–342.4 mg/g. Fig. 9(a) showed the influence of loading amount of 2,4,6-TCP on the catalytic degradation of EDA@nFe$_3$O$_4$-2,4,6-TCP-Fe(III)-H_2O_2 system. The results showed when the 2,4,6-TCP loading amount on EDA@nFe$_3$O$_4$ less than 122.2 mg/g, the 2,4,6-TCP loaded on EDA@nFe$_3$O$_4$ can be completely degraded within 5 min. For those 2,4,6-TCP loading amount on EDA@nFe$_3$O$_4$ larger than 122.2 mg/g, longer time (30 min) and more Fe^{3+} (200 μL) as well as H_2O_2 (50 μL) would be needed to obtain a degradation percentage over 90% (Fig. 9(a), inset). Fig. 9(b) shows the effect of the solution pH values on the catalytic degradation of EDA@nFe$_3$O$_4$-2,4,6-TCP-Fe(III)-H_2O_2 system. In the range of pH value at pH 3.0–8.0, the degradation rate of 2,4,6-TCP is nearly 100%

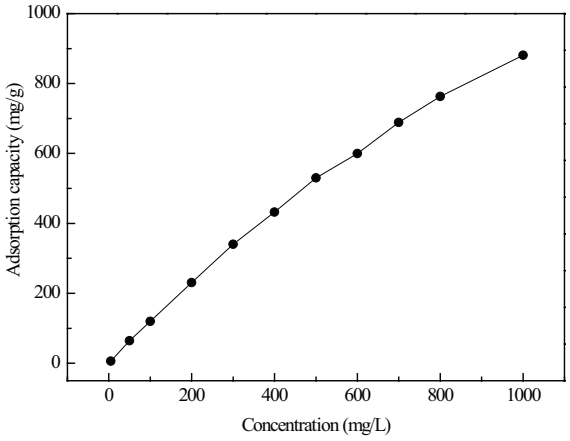

Fig. 8. Adsorption isotherms of 2,4,6-TCP on the EDA@nFe$_3$O$_4$.

Table 1
Pseudo-second-order rate equations and constants of EDA@nFe$_3$O$_4$

C_0 (mg/L)	Equations	k_2 (g/(mg min))	q_e (mg/g)	$q_{e,cal}$ (mg/g)	$k_2q_e^2$ (mg/(g min))	R^2
50	t/q_t = 0.0159t + 0.0165	0.0153	62.2	62.9	60.6	0.9997
200	t/q_t = 0.0042t + 0.0012	0.0147	232.8	238.1	833.3	0.9995
500	t/q_t = 0.0018t + 0.00022	0.0147	545.8	555.6	4,545	0.9996

Table 2
The 2,4,6-TCP adsorption isotherm equations and parameters of Langmuir and Freundlich models

Model	Isotherm	Parameters	q^{ea} (mg/L)	R^2
Langmuir	C_e/q_e = 0.0011C_e + 0.4407	K = 0.027 L/mg q_m^c = 909.1 mg/g	902.5	0.933
Freundlich	logq_e = 0.4692logC_e + 1.8155	K_F = 65.39 1/n = 0.523		0.997

[a]q^e and q^c are the experimental adsorption capacity, respectively.

in 5 min, which is a much wider pH range than that of common Fenton reaction system. For comparing, the adsorption property of the pure Fe_3O_4 was investigated, however, the adsorption efficiency was at only 2.1% even the initial concentration of 2,4,6-TCP at 5.00 mg/L, that is, loading amount at 0.13 mg/g. Further, in situ degradation of 2,4,6-TCP on post-adsorption Fe_3O_4 was also carried out and the degradation percentage was found at 30.2%, by adding 100 μL of Fe^{3+} solution at concentration of 10^{-3} mol/L, and 20 μL of 30% H_2O_2, under pH at 3.0, which was much lower than that of the EDA@nFe$_3$O$_4$-2,4,6-TCP-Fe(III)-H_2O_2 system. This might be due to the fact that the excess amino group on the surface of post-adsorption EDA@nFe$_3$O$_4$ can be further combined with Fe(III) via coordinating bonds to form a Fenton-like heterogeneous catalytic system, thus weakening the pH influence on catalytic degradation reaction.

3.4. Reusability investigation

The reusable of the EDA@nFe$_3$O$_4$ was evaluated by comparing the adsorption as well as degradation efficiency. The post-absorbed EDA@nFe$_3$O$_4$ was extracted with 1% NaOH methanol solution for 30 min, and for another adsorption to get the next adsorption efficiency. The results were shown in Fig. 10(a). After degradation of 2,4,6-TCP, the used EDA@nFe$_3$O$_4$ can also be reused for adsorption, followed by in situ degradation of 2,4,6-TCP, directly. The results for those of the initial concentration of 50.0 mg/L are shown in Fig. 10(b). The results indicated that EDA@nFe$_3$O$_4$ could be used for at least five cycles with a loss of less than 3.2% upon recovery on average. No obvious decrease in the adsorption capacity or degradation efficiency was found. The SEM or TEM image of EDA-nFe$_3$O$_4$ after cyclic adsorption and degradation were examined, shown in Figs. 11(a) and (b), respectively. It revealed that the EDA@nFe$_3$O$_4$ particles were multidispersed without much change in morphology. These results showed that the EDA@nFe$_3$O$_4$ was stable and could be recycled.

3.5. Radicals trapping experiences

In order to identify the major active species in the photodegradation process, radical-trapping measurements were also performed, according to literature reports [34–37]. The results are displayed in Fig. 12. The photodegradation of 2,4,6-TCP was greatly inhibited (from 92.2% to 5.5%) by the addition of 1 mmol/L *tert*-butanol (a hydroxyl radical scavenger)

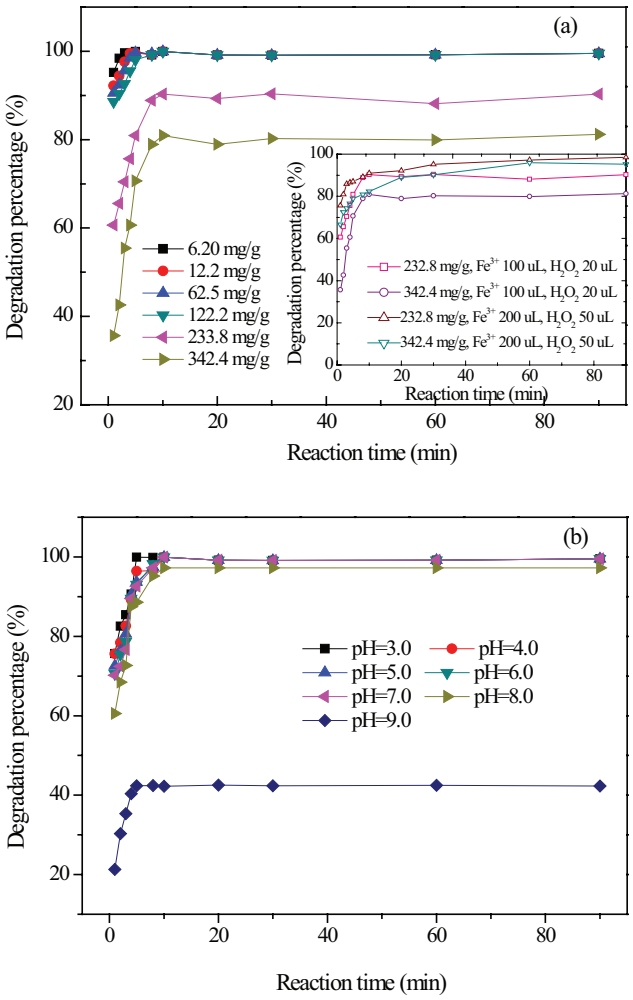

Fig. 9. Effect of loading amount of (a) 2,4,6-TCP and (b) solution pH value on the EDA@nFe$_3$O$_4$ for EDA@nFe$_3$O$_4$-2,4,6-TCP-Fe(III)-H_2O_2 catalytic degradation system.

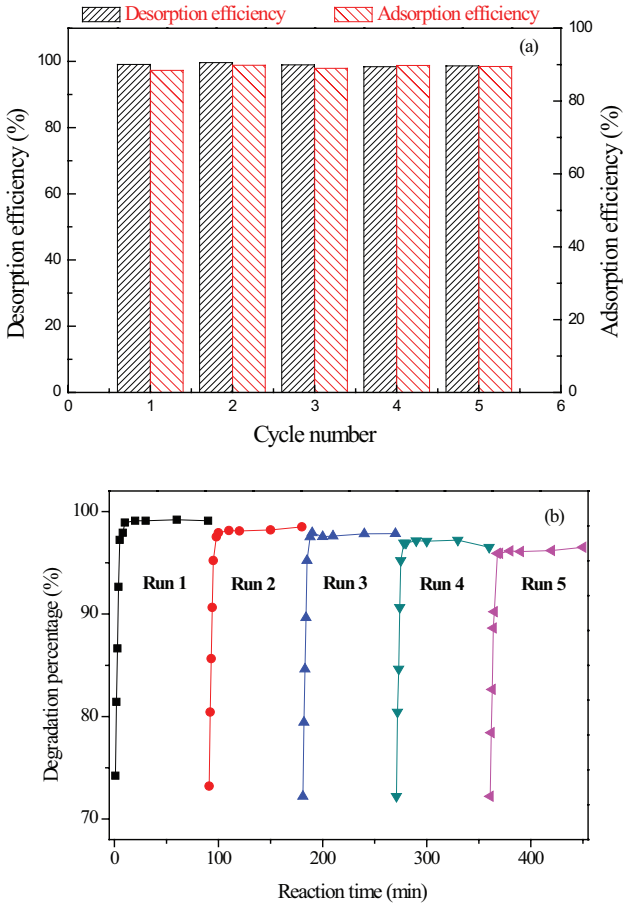

Fig. 10. Reusability of EDA@nFe$_3$O$_4$ (a) after adsorption and (b) after degradation.

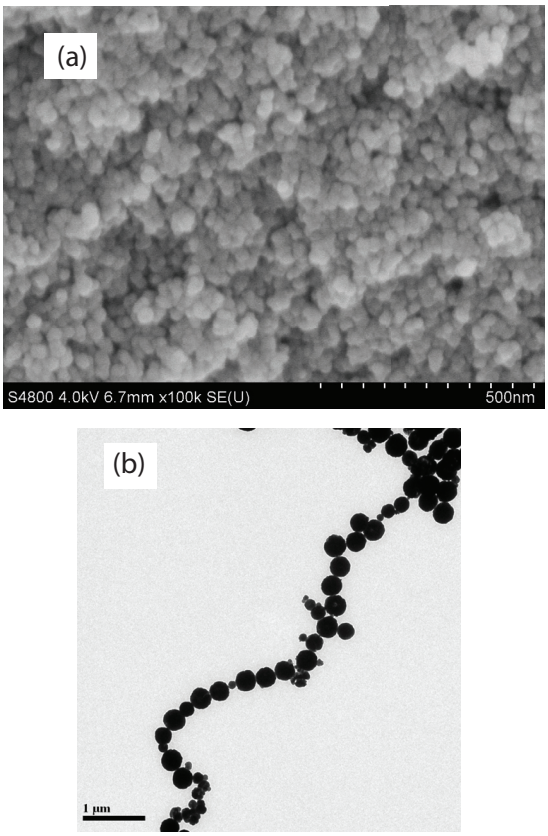

Fig. 11. (a) SEM and (b) TEM image of EDA@nFe$_3$O$_4$ after cyclic adsorption and degradation for five times.

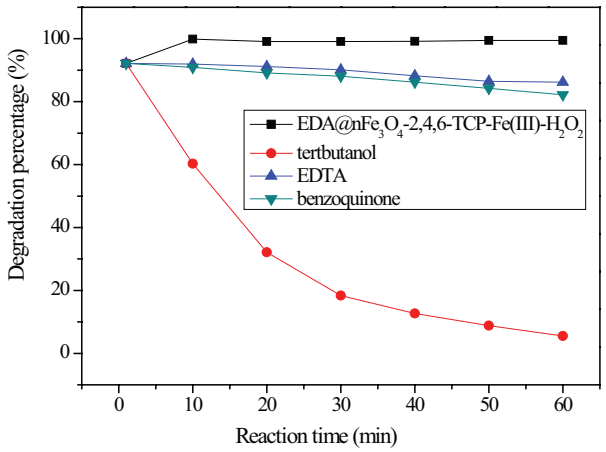

Fig. 12. Plots of active species trapped in the system for the photodegradation of 2,4,6-TCP using EDA@nFe$_3$O$_4$-2,4,6-TCP-Fe(III)-H_2O_2 catalytic degradation system.

for 90 min, indicating that the •OH radicals are the dominant active oxidizing species in the photoreaction process, while the 2,4,6-TCP degradation was slightly inhibited with the use of 1 mmol/L of Na_2-EDTA (a hole scavenger) and benzoquinone (a superoxide anion radical scavenger, $O_2^{\bullet-}$). Therefore, the photogenerated holes and $O_2^{\bullet-}$ are the minor reactive species contributing to the oxidative degradation of 2,4,6-TCP.

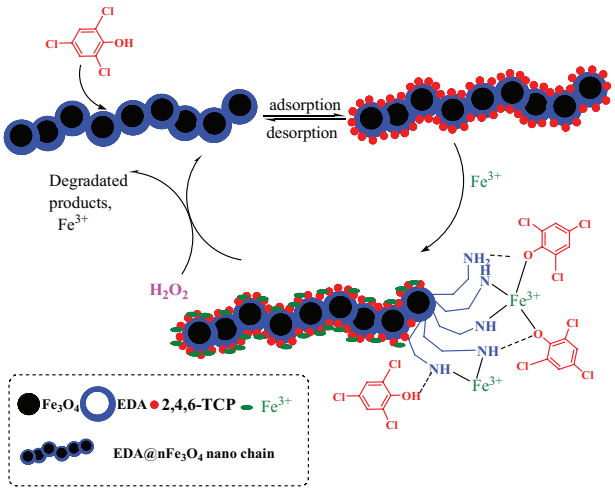

Fig. 13. Presumed mechanism of absorption and in situ degradation of 2,4,6-TCP on the EDA@nFe$_3$O$_4$.

3.6. Presumed mechanism

Presumed mechanism is given in Fig. 13. The adsorption of 2,4,6-TCP on EDA@nFe$_3$O$_4$ can be realized via hydrogen bonds between hydroxyl group (–OH) of 2,4,6-TCP and the amino groups (–NH_2) at the surface of EDA@nFe$_3$O$_4$ in the pH range at 4.0–8.0. Desorption of 2,4,6-TCP can be realized in 1% NaOH methanol solution for the regeneration of EDA@nFe$_3$O$_4$ reversibly. The post-adsorbed EDA@nFe$_3$O$_4$ can be further combined with Fe(III) via coordinating bonds. With H_2O_2 being added, Fenton-like heterogeneous catalytic system can be formed and in situ degradation of 2,4,6-TCP can be finally realized. The EDA@nFe$_3$O$_4$ can be released for recycling.

4. Conclusion

An EDA-functionalized nano-Fe$_3$O$_4$ nanochain was synthesized by a facile one-pot solvothermal method. It was applied for adsorption and in situ degradation of 2,4,6-TCP in aqueous solution. The adsorption processes reach the equilibrium within 5 min and the adsorption capacity is found to be 902.5 mg/g with the initial concentration of 2,4,6-TCP at 1,000 mg/L. The kinetic data are well fitted to the pseudo-second-order model, while the adsorption thermodynamic studies suggest that the adsorption processes fit the Freundlich isotherms well. In situ degradation of 2,4,6-TCP via Fenton-like reaction under visible light can be realized with a wider pH range (3.0–8.0) and high degradation percentage, that is, almost 100% within 5 min with the loading amount of 2,4,6-TCP at 6.20–122.2 mg/g. The EDA@nFe$_3$O$_4$ can be reused after regeneration. It is a potential effective and reusable material for adsorption and degradation of 2,4,6-TCP.

Acknowledgments

The authors would like to thank the National Natural Science Foundation of China (LY14B04003), and also like to thank the National Natural Science Foundation of Zhejiang Province (LY14B04003), the National Natural Science Foundation of Ningbo (2014A610092), the National College

Students' innovation and entrepreneurship training program (201513022009), the Xinmiao Students' innovation training program of Zhejiang Province (2015R401181) for the financial support.

References

[1] G. Cagnetta, J. Robertson, J. Huang, K.L. Zhang, G. Yu, Mechanochemical destruction of halogenated organic pollutants: a critical review, J. Hazard. Mater., 313 (2016) 85–102.

[2] J.Q. Guo, C.H. Wu, S.L. Lv, D.S. Lu, C. Feng, X.J. Qi, W.J. Liang, X.L. Chang, H. Xu, G.Q. Wang, Z.J. Zhou, Associations of prenatal exposure to five chlorophenols with adverse birth outcomes, Environ. Pollut., 214 (2016) 478–484.

[3] J.L. Fan, J. Zhang, C.L. Zhang, L. Reb, Q.Q. Shi, Adsorption of 2,4,6-trichlorophenol from aqueous solution onto activated carbon derived from loosestrife, Desalination, 267 (2011) 139–146.

[4] P. Strachowski, M. Bystrzejewski, Comparative studies of sorption of phenolic compounds onto carbon-encapsulated iron nanoparticles, carbon nanotubes and activated carbon, Colloids Surf., A, 467 (2015) 113–123.

[5] M.M. Machawe, M.T. Justice, A.M.M. Titus, B.M. Bhekie, Adsorption of 2,4,6-trichlorophenol and ortho-nitrophenol from aqueous media using surfactant-modified clinoptilolite-polypropylene hollow fibre composites, Water Air Soil Pollut., 223 (2012) 1555–1569.

[6] M.S. Bilgili, Adsorption of 4-chlorophenol from aqueous solutions by xad-4 resin: isotherm, kinetic, and thermodynamic analysis, J. Hazard. Mater., 137 (2006) 157–164.

[7] S. Mubari, A. Saeed, M.M. Athar, M. Iqbal, Characterization and mechanism of the adsorptive removal of 2,4,6-trichlorophenol by biochar prepared from sugarcane baggase, J. Ind. Eng. Chem., 33 (2016) 115–121.

[8] H.Y. Shen, Z.X. Chen, Z.H. Li, M.Q. Hu, X.Y. Dong, Controlled synthesis of 2,4,6-trichlorophenol-imprinted amino-functionalizednano-Fe_3O_4-polymer magnetic composite for highly selective adsorption, Colloids Surf., A, 481 (2015) 439–450.

[9] C.M. Su, Environmental implications and applications of engineered nanoscale magnetite and its hybrid nanocomposites: a review of recent literature, J. Hazard. Mater., 322 (2017) 48–84.

[10] Y.G. Zhao, X.H. Chen, S.D. Pan, H. Zhu, H.Y. Shen, M.C. Jin, Self-assembly of surface bisphenol A-imprinted core-shell nanoring amino-functionalized superparamagnetic polymer, J. Mater. Chem. A, 1 (2013) 11648–11658.

[11] H.Y. Shen, S.D. Pan, Y. Zhang, X.L. Huang, H.X. Gong, A new insight on the adsorption mechanism of amino-functionalized nano-Fe_3O_4 magnetic polymers in Cu(II), Cr(VI) co-existing water system, Chem. Eng. J., 183 (2012) 180–191.

[12] H.Y. Shen, J.L. Chen, H.F. Dai, L.B. Wang, M.Q. Hu, Q.H. Xia, New insights into the sorption and detoxification of chromium(VI) by tetraethylenepentamine functionalized nano-sized magnetic polymer adsorbents: mechanism and pH effect, Ind. Eng. Chem. Res., 52 (2013) 12723–12732.

[13] S.D. Pan, H.Y. Shen, Q.H. Xu, J. Luo, M.Q. Hu, Surface mercapto engineered magnetic Fe_3O_4 nanoadsorbent for the removal of mercury from aqueous solutions, J. Colloid Interface Sci., 365 (2012) 204–212.

[14] H.Y. Shen, Z.X. Chen, Z.H. Li, M.Q. Hu, X.Y. Dong, Q.H. Xia, Controlled synthesis of 2,4,6-trichlorophenol-imprinted amino-functionalized nano-Fe_3O_4-polymer magnetic composite for highly selective adsorption, Colloids Surf., A, 481 (2015) 439–450.

[15] S.D. Pan, Y. Zhang, H.Y. Shen, M.Q. Hu, An intensive study on the magnetic effect of mercapto-functionalized nano magnetic Fe_3O_4 polymers and their adsorption mechanism for the removal of Hg(II) from aqueous solution, Chem. Eng. J., 210 (2012) 564–574.

[16] N.S. Goldstein, D. Meyerstein, Comments on the mechanism of the "Fenton-like" reaction, Acc. Chem. Res., 32 (1999) 547–549.

[17] E. Nevens, J. Baevenes, A review of classic Fenton's peroxidation as an advanced oxidation technique, J. Hazard. Mater., 98 (2003) 33–50.

[18] B.X. Cai, Y.W. Chen, Basical Chemistry Experiments, Science Press, Beijing, China, 2001.

[19] J. Febrianto, A.N. Kosasih, J. Sunarso, Y.H. Ju, N. Indraswati, S. Ismadji, Equilibrium and kinetic studies in adsorption of heavy metals using biosorbent: a summary of recent studies, J. Hazard. Mater., 162 (2009) 616–645.

[20] H. Deng, X.L. Li, Q. Peng, X. Wang, J.P. Chen, Y.D. Li, Monodisperse magnetic single-crystal ferrite microspheres, Angew. Chem. Int. Ed., 44 (2005) 2782–2785.

[21] Y.S. Ho, Review of second-order models for adsorption systems, J. Hazard. Mater., 136 (2006) 681–689.

[22] S.H. Huang, D.H. Chen, Rapid removal of heavy metal cations and anions from aqueous solutions by an amino-functionalized magnetic nano-adsorbent, J. Hazard. Mater., 163 (2009) 174–179.

[23] K.Y. Foo, B.H. Hameed, Review: insights into the modeling of adsorption isotherm systems, Chem. Eng. J., 156 (2010) 2–10.

[24] B. Liu, W. Zhang, F.K. Yang, H.L. Feng, X.L. Yang, Facile method for synthesis of Fe_3O_4@polymer microspheres and their application as magnetic support for loading metal nanoparticles, J. Phys. Chem. C, 115 (2011) 15875–15884.

[25] Y.G. Zhao, H.Y. Shen, S.D. Pan, M.Q. Hu, Synthesis, characterization and properties of ethylene-diamine-functionalized Fe_3O_4 magnetic polymers for removal of Cr(VI) in wastewater, J. Hazard. Mater., 182 (2010) 295–302.

[26] M. Czaplicka, Sources and transformations of chlorophenols in the natural environment, Sci. Total Environ., 322 (2004) 21–39.

[27] Y. Zhang, S.D. Pan, H.Y. Shen, M.Q. Hu, Amino-functionalized nano-size composite materials for dispersive solid phase extraction of phosphate in water samples, Anal. Sci., 28 (2012) 887–892.

[28] H.Y. Shen, B.W. Liu, Q. Xiang, C.C. Wang, S.Q. Mao, Highly selective amino-functionalized magnetic molecularly imprinted polymers: absorbents for dispersive solid phase extraction and trace level analysis of chlorophenols in seawater, RSC Adv., 6 (2016) 81330–81340.

[29] Y.G. Zhao, H.Y. Shen, S.D. Pan, M.Q. Hu, Q.H. Xia, Preparation and characterization of amino-functionalized nano-Fe_3O_4 magnetic polymer adsorbents for removal of chromium(VI) ions, J. Mater. Sci., 49 (2010) 5291–5301.

[30] J. Chen, M.A. Hamon, H. Hu, Y. Chen, A.M. Rao, P.C. Eklund, R.C. Haddon, Solution properties of single-walled carbon nanotubes, Science, 282 (1998) 95–98.

[31] L. Zhou, L. Ji, P.C. Ma, Y. Shao, H. Zhang, W. Gao, Y. Li, Development of carbon nanotubes/$CoFe_2O_4$ magnetic hybrid material for removal of tetrabromobisphenol A and Pb(II), J. Hazard. Mater., 265 (2014) 104–114.

[32] G. Crini, H.N. Peindy, F. Gimbert, C. Robert, Removal of C.I. Basic Green 4 (Malachite Green) from aqueous solutions by adsorption using cyclodextrin-based adsorbent: kinetic and equilibrium studies, Sep. Purif. Technol., 53 (2007) 97–110.

[33] A. Ozcan, A.S. Ozcan, Adsorption of Acid Red 57 from aqueous solutions onto surfactant-modified sepiolite, J. Hazard. Mater., 125 (2005) 252–259.

[34] X.H. Gao, H.B. Wu, L.X. Zheng, Y.J. Zhong, Y. Hu, X.W. Lou, Formation of mesoporous heterostructured $BiVO_4/Bi_2S_3$ hollow discoids with enhanced photoactivity, Angew. Chem. Int. Ed., 53 (2014) 5917–5921.

[35] R. Qiao, M.M. Mao, E.L. Hu, Y.J. Zhong, J.Q. Ning, Y. Hu, Facile formation of mesoporous $BiVO_4$/Ag/AgCl heterostructured microspheres with enhanced visible-light photoactivity, Inorg. Chem., 54 (2015) 9033–9039.

[36] S.L. Wang, J.J. Li, X.D. Zhou, C.C. Zheng, J.Q. Ning, Y.J. Zhong, Y. Hu, Facile preparation of 2D sandwich-like CdS nanoparticles/nitrogen-doped reduced graphene oxide hybrid nanosheets with enhanced photoelectrochemical properties, J. Mater. Chem. A, 2 (2014) 19815–19821.

[37] A. Etogo, E.L. Hu, C.M. Zhou, Y.J. Zhong, Y. Hu, Z.L. Hong, Facile fabrication of mesoporous $BiOCl/(BiO)_2CO_3/Bi_2O_3$ ternary flower-like heterostructured microspheres with high visible-light-driven photoactivity, J. Mater. Chem. A, 3 (2015) 22413–22420.